JOURNAL OF SPACECRAFT AND ROCKETS
Vol. 44, No. 4, July–August 2007

Solar Sail Kinetic Energy Impactor Trajectory Optimization for an Asteroid-Deflection Mission

Bernd Dachwald*
DLR, German Aerospace Center, 51170 Cologne, Germany
and
Bong Wie†
Arizona State University, Tempe, Arizona 85287

DOI: 10.2514/1.22586

A fictional asteroid-mitigation problem created by AIAA assumes that a 200-m near-Earth asteroid, detected on 04 July 2004 and designated as 2004 WR, will impact the Earth on 14 January 2015. Adopting this example scenario, we show that solar sail spacecraft that impact the asteroid with a very high relative velocity are a realistic near-term option for mitigating the impact threat from near-Earth asteroids. The proposed mission requires several kinetic energy impactor solar sail spacecraft. Each kinetic energy impactor consists of a 160 × 160 m, 168-kg solar sail and a 150-kg impactor. Because of their large ΔV capability, solar sailcraft with a relatively modest characteristic acceleration of 0.5 mm/s^2 can achieve an orbit that is retrograde to the target orbit within less than about 4.5 years. Before impacting 2004 WR at its perihelion of about 0.75 AU, each impactor is to be separated from its solar sail. With a relative impact velocity of about 81 km/s, each impactor will cause a conservatively estimated Δv of about 0.35 cm/s in the trajectory of the target asteroid, largely due to the impulsive effect of material ejected from the newly formed crater. The deflection caused by a single impactor will increase the Earth-miss distance by about 0.7 Earth radii. Several sailcraft will therefore be required for consecutive impacts, to increase the total Earth-miss distance to a safe value. In this paper, we elaborate on a potential mission scenario and investigate trade-offs between different mission parameters; for example, characteristic acceleration, sail temperature limit, hyperbolic excess energy for interplanetary insertion, and optical solar sail degradation.

Introduction

NEAR-EARTH objects (NEOs) are asteroids and short-period comets with orbits that intersect or pass near the orbit of Earth (perihelion $r_p \leq 1.3$ AU). Currently (September 2006), 839 near-Earth asteroids (NEAs) with an absolute magnitude $H \leq 18$ (diameter $d \gtrsim 1$ km) are known [1], but the entire population contains perhaps more than 1000 objects of this size [2]. All NEAs with an Earth minimum orbit intersection distance (MOID) less than or equal to 0.05 AU and $H \leq 22$ ($d \gtrsim 200$ m) are termed potentially hazardous asteroids (PHAs). There are currently 799 known PHAs, 162 of them with $H \leq 18$ ($d \gtrsim 1$ km) [1]. They pose a significant hazard to human civilization and to life on Earth. It is widely accepted today that NEO impacts have caused at least one mass extinction (65 million years ago at the Cretaceous/Tertiary boundary), and they are suspected to have caused several global catastrophes before that [3,4]. A 2-km object is capable of causing catastrophic alteration of the global ecosystem [5]. Ocean impacts of even smaller objects are of some concern, because the destructive potential caused by the resulting tsunamis may be above that from a land impact [5,6]. Even objects that do not intersect Earth's orbit may evolve into Earth-crossers, because their orbits are chaotic, having a relatively short dynamic lifetime of about 10^7 years [7–9]. Although this paper is about a fictional scenario, one day it might become necessary to prevent a specific object from impacting the Earth by nudging it out of its orbit. The probability of major impacts with severe effects for humanity is low, but not zero. This paper presents a realistic near-term solution to mitigate this threat.

Mission Scenario

A fictional asteroid-mitigation problem was created by AIAA for the 2004/2005 AIAA Foundation Undergraduate Team Space Design Competition: on 04 July 2004, the NASA/Jet Propulsion Laboratory near-Earth asteroid-tracking (NEAT) camera at the Maui Space Surveillance Site discovered an Apollo asteroid with an estimated diameter of 0.205 km, designated 2004WR. This asteroid has been assigned a Torino Impact Scale rating of 9.0 on the basis of subsequent observations that indicate a 95% probability that 2004WR will impact the Earth. The expected impact will occur in the southern hemisphere on 14 January 2015, causing catastrophic damage throughout the Pacific region. The mission task was to design a space system that can rendezvous with 2004WR in a timely manner, inspect it, and remove the hazard to Earth by changing its orbit and/or destroying it. The classical orbital elements of 2004WR in the J2000 heliocentric ecliptic reference frame are

$$\text{Epoch} = 53200\,\text{TDB}\ (14\ \text{July}\ 2004) \qquad a = 2.15374076\ \text{AU}$$
$$e = 0.649820926 \qquad i = 11.6660258\ \text{deg}$$
$$\omega = 66.2021796\ \text{deg} \qquad \Omega = 114.4749665\ \text{deg}$$
$$M = 229.8987151\ \text{deg}$$

It was further assumed that 2004WR is an S-class (stony silicate) asteroid with a density of 2720 kg/m^3 and that its estimated mass is 1.1×10^{10} kg. This AIAA problem is very similar to other fictional asteroid-mitigation problems, called defined threat (DEFT) scenarios, that have been created for the 2004 Planetary Defense Conference. One of the four DEFT scenarios is about mitigating a fictional 200-m asteroid with a predicted impact date of 29 February 2016.

Presented as Paper 6176 at the AIAA Guidance, Navigation, and Control Conference, San Francisco, CA, 15–18 August 2005; received 20 January 2006; revision received 28 September 2006; accepted for publication 18 December 2006.

*Scientist, currently at Mission Operations Section, Oberpfaffenhofen, 82234 Wessling, Germany; bernd.dachwald@dlr.de. Member AIAA.

†Professor, Department of Mechanical and Aerospace Engineering; bong.wie@asu.edu. Associate Fellow AIAA.

The simplest approach to deflect a NEA is to impact it with a massive projectile at a high relative velocity. The change in the object's Earth-miss distance due to the impact depends on the time between the kinetic energy impactor's (KEI's) impact and the object's Earth impact, the lead time Δt_L, and the velocity change Δv of the asteroid caused by the impactor. In rough terms, the KEI's impact causes an along-track position shift of [10,11]

$$\Delta x = 3\Delta t_L \Delta v \tag{1}$$

Thus, a Δv of 0.1 cm/s provides a Δx of about 100 km in 1 year.

A successful asteroid-deflection mission will require accurate modeling and prediction of the velocity change caused by the impactor. The effective impulse imparted to the asteroid will be the sum of the pure kinetic impulse (linear momentum) of the impactor plus the impulse due to the "thrust" of material being ejected from the impact crater. The last term can be very significant (even dominant), but its magnitude depends strongly upon the density and yield strength of the material of which the asteroid is composed, as well as the mass and relative velocity of the impactor. For example, a head-on collision (at a relative velocity of $v_{\text{imp}} = 80$ km/s) of a 150-kg impactor on a 200-m S-class asteroid (with a density of 2720 kg/m^3) yields a pure kinetic-impact Δv of approximately 0.1 cm/s. If the asteroid is composed of hard rock, then the modeling of crater ejecta impulse from previous studies would predict an additional Δv of 0.2 cm/s, which is double the pure kinetic-impact Δv [11,12]. If the asteroid is composed of soft rock, however, the previous studies would instead predict an additional Δv of 0.6 cm/s, which is about six times the pure kinetic-impact Δv. An accurate modeling and prediction of the ejecta impulse for various asteroid compositions is therefore a critical issue for all kinetic-impact approaches. A practical concern of any kinetic-impact approach is the risk that the impact could result in the fragmentation of the asteroid, which could substantially increase the damage upon Earth impact [13]. The energy required to fragment an asteroid depends critically upon its composition and structure. For example, for a 200-m asteroid composed largely of ice, the disruption energy is approximately 3.4×10^{10} J. Because the kinetic energy of a 150-kg impactor at a relative velocity of 80 km/s would be 4.8×10^{11} J, the ice asteroid would likely fragment [14]. If the asteroid is composed largely of silicates, it would have a disruption energy of approximately 2.3×10^{12} J, about five times larger than the kinetic energy delivered by the impactor; this asteroid would likely stay intact [14]. Therefore, further studies are needed to optimize impactor size, relative impact velocity, and the total number of impactors as functions of the asteroid's size and composition, to ensure that the impact does not cause fragmentation.

Our proposed mission scenario employs a solar sail to deliver impactors to an orbit retrograde to the asteroid's orbit, from the point from which they impact the target with very high kinetic energy. The use of solar sails to achieve impacts from retrograde orbits was first proposed (and elaborated in a more general way) by McInnes [15,16]. Wie [14,17] employed the same idea for AIAA's fictional asteroid-deflection problem and made a preliminary conceptual mission design. In [18], Dachwald and Wie made a more rigorous trajectory-optimization study for this mission. Based on [18], this paper focuses on rigorous trajectory optimization for AIAA's fictional asteroid-deflection problem [14,17]. The proposed mission scenario comprises three phases (see Fig. 1): 1) a spiraling-in phase, 2) an orbit-cranking phase to an orbit that is retrograde to the asteroid's one, and 3) a final retrograde orbit phase before impacting the target asteroid at its perihelion with maximum efficiency.

A head-on collision yields an impact velocity of more than 80 km/s, which is much higher than the typical impact velocity of about 10 km/s of prograde missions such as NASA's Deep Impact mission [19] or ESA's Don Quijote mission [20]. The impactor is to be separated from the solar sail before impacting the target asteroid, because of the extremely demanding terminal guidance and targeting requirements (the accuracy of the impactor trajectory must be much better than 100 m at a relative velocity of more than 80 km/s). For the present scenario, several KEI sailcraft will be required to increase the Earth-miss distance to a safe value. For larger asteroids, the impactor may not have to be separated from the solar sail, but the complete solar sail spacecraft could be designed to impact, thereby increasing the impacting mass and, thus, the resulting Δv.

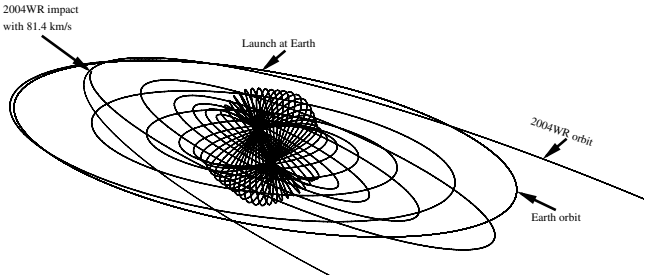

Fig. 1 Proposed mission scenario.

Our baseline KEI consists of a 160×160 m, 168-kg solar sail and a 150-kg impactor, the solar sail being based on the sound engineering of the scalable sailcraft design by ATK Space Systems [21–28]. Note that a variety of solar sail missions require 160-m solar sails and the associated solar sail technologies are being developed. In particular, a 160-m solar sail will be required for the Solar Polar Imager (SPI) mission, which is one of the sun–Earth connection solar sail roadmap missions currently envisioned by NASA [21].

The critical technologies required for the proposed mission include: 1) deployment and control of a 160×160 m solar sail, 2) development of a solar sail and a microspacecraft bus that is able to withstand the extreme space environment at less than only 0.25 AU from the sun, 3) autonomous precision navigation, terminal guidance, and targeting, and 4) accurate impact-crater ejecta modeling and Δv prediction. A 160×160 m solar sail is currently not available. However, a 20×20 m solar sail structure was already deployed on the ground in a simulated gravity-free environment at DLR in December 1999, a 40×40 m solar sail is being developed by NASA and industries for a possible flight-validation experiment within 10 years; thus, a 160×160 m solar sail is expected to be available within about 20 years of a sharply pursued technology development program.

Simulation Model

In this paper, the standard nonperfectly reflecting solar radiation pressure (SRP) force model by Wright [29] is employed. For a detailed description of this model, the reader is referred to [30].

In addition to the gravitational forces of all celestial bodies and the SRP force, many disturbing forces influence the motion of solar sails in space; they are caused, for example, by the solar wind, the finiteness of the solar disk, the reflected light from close celestial bodies, and the aberration of solar radiation (Poynting–Robertson effect). Furthermore, a real solar sail bends and wrinkles, depending on the actual solar sail design. Finally, for a mission that is to target the center of mass of a 200-m object with a relative velocity of more than 80 km/s, relativistic corrections may have to be applied for the final targeting phase. All of these issues have to be considered for high-precision trajectory determination and control, as is required for this mission. For mission feasibility analysis, however, as is done within this paper, the following simplifications can be made:

1) The solar sail is moving under the sole influence of solar gravitation and radiation.

2) The solar sail attitude can be changed instantaneously.

In a heliocentric inertial right-handed Cartesian coordinate frame $\mathcal{I} = \{\boldsymbol{e}_x, \boldsymbol{e}_y, \boldsymbol{e}_z\}$, the equations of motion for a solar sail are

$$\dot{\boldsymbol{r}} = \boldsymbol{v}, \qquad \dot{\boldsymbol{v}} = -\frac{\mu}{r^3}\boldsymbol{r} + \boldsymbol{a}_{\text{SRP}} \tag{2}$$

where $\boldsymbol{r} = (r_x, r_y, r_z)$ is the solar sail position, $\boldsymbol{v} = (v_x, v_y, v_z)$ is the solar sail velocity, μ is the sun's gravitational parameter, and $\boldsymbol{a}_{\text{SRP}}$ is the SRP acceleration.

Trajectory-Optimization Methods

Local Steering Laws

Although local steering laws (LSLs) are not trajectory-optimization methods in the narrower sense, because they do not yield locally optimal trajectories, they give the locally optimal thrust directions to change some specific osculating orbital element of the spacecraft with a locally maximum rate. The LSLs for the semimajor axis a can be written as $\mathrm{d}a/\mathrm{d}t = \boldsymbol{k}_a \cdot \boldsymbol{a}_{\mathrm{SRP}}$ and the LSLs for the inclination i can be written as $\mathrm{d}i/\mathrm{d}t = \boldsymbol{k}_i \cdot \boldsymbol{a}_{\mathrm{SRP}}$. It is clear that to decrease the semimajor axis with a maximum rate, the thrust vector has to be along the direction $-\boldsymbol{k}_a$ (local steering law $\mathcal{L}_{a^-}$). To increase the inclination with a maximum rate, the thrust vector has to be along the direction $\boldsymbol{k}_i$ ($\mathcal{L}_{i^+}$). Unlike for other spacecraft, however, for which the thrust vector can be directed into any desired direction, the SRP force vector of a solar sail is constrained to lie on a "bubble" that is directed away from the sun [30]. Therefore, when using LSLs, the projection of the SRP force vector onto the respective $\boldsymbol{k}$ vector has to be maximized.

Evolutionary Neurocontrol: A Global Trajectory-Optimization Method

Within this paper, evolutionary neurocontrol (ENC) was also used to calculate the trajectories. This method is based on a combination of artificial neural networks (ANNs) with evolutionary algorithms (EAs). For a description of this method, the reader is referred to [31–33]. ENC was implemented within a low-thrust trajectory-optimization program called *intelligent trajectory optimization using neurocontroller evolution* (InTrance). InTrance is a global trajectory-optimization method that requires only the target body/state and intervals for the initial conditions as input to find a good solution for the specified problem. It works without an initial guess and does not require the attendance of a trajectory-optimization expert. Because InTrance does not use any gradient information (as is characteristic of evolutionary algorithms), it does not permit a fast convergence in the nearness of an optimum and therefore cannot locate optimal solutions exactly, but only near-optimal solutions. Although InTrance searches the solution space very efficiently, it might (for difficult search space topologies) miss the (near-) global optimum and also converge to a (near-) local optimum.

Results

Optimization of the Baseline Mission Scenario

Overall Description

The baseline mission scenario foresees a nonperfectly reflecting solar sail with a characteristic acceleration (SRP acceleration acting on a solar sail that is oriented perpendicular to the sun line at 1 AU) of $a_c = 0.5\ \mathrm{mm/s^2}$, a sail temperature limit of $T_{\mathrm{lim}} = 240°\mathrm{C}$, and interplanetary insertion at Earth with zero hyperbolic excess energy, $C_3 = 0\ \mathrm{km^2/s^2}$. Generally, orbits with $i < 90$ deg are termed prograde orbits, and orbits with $i > 90$ deg are termed retrograde orbits. It was first found by Wright [34,35] and further examined by Sauer [36] that the best way to attain a retrograde orbit with a solar sail is to first spiral inwards to a solar distance that is given by the temperature limits T_{lim} of the solar sail and the spacecraft, then to use the large available SRP to crank the orbit. However, although the sail temperature depends not only on the solar distance but also on the pitch angle, as will be seen later, Sauer used a minimal solar distance r_{lim} instead of a temperature limit T_{lim}. During the orbit-cranking phase, the local steering law $\mathcal{L}_{i^+}$ is applied until the desired inclination is reached. To simplify the terminology within this paper, we speak of a retrograde orbit when the orbital angular momentum vector of the spacecraft $\boldsymbol{h}$ and the target $\boldsymbol{h}_T$ are antiparallel; that is, $\angle(\boldsymbol{h}, -\boldsymbol{h}_T) = 0$ deg. Using local steering laws, the strategy to attain such a retrograde orbit divides the trajectory into two well-defined phases: 1a spirals inwards until the optimum solar distance for cranking the orbit is reached using local steering law $\mathcal{L}_{a^-}$ (the inclination stays constant during phase 1a), and 1b cranks the orbit until the orbit is retrograde using local steering law $\mathcal{L}_{a^+}$ (the semimajor axis stays constant during phase 1b). Therefore, it might become necessary to change the ascending node of the orbit so that the inclination change is ≤ 180 deg.

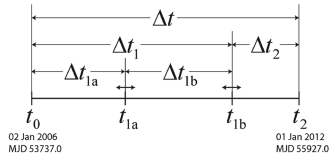

Fig. 2 Mission timeline.

Phases 1a and 1b can be regarded as a single phase, phase 1 (later, using InTrance, phase 1 will be optimized in one pass). Phase 1 has to be followed by a phase 2, for which no simple LSL exists. The goal of phase 2 is to impact the target head-on with maximum relative velocity. The time that is spent for the different phases is then $\Delta t = \Delta t_1 + \Delta t_2$ with $\Delta t_1 = \Delta t_{1a} + \Delta t_{1b}$ ($\Delta t_{1a} = t_{1a} - t_0$, $\Delta t_{1b} = t_{1b} - t_{1a}$, and $\Delta t_2 = t_2 - t_{1b}$), with the constraint that the launch date and the impact date are assumed fixed within this paper (see Fig. 2). As we will see later from the InTrance solutions, using local steering laws and patching the solutions of phases 1a, 1b, and 2 together yields a suboptimal solution, because a globally optimal trajectory has a smooth transition between the three phases, also changing the inclination slightly during phases 1a and 2, whenever the sailcraft is close to the nodes. Therefore, we define t_{1b}, the end of phase 1, as follows. Let $\Delta i_{\boldsymbol{T}} = |i_{\boldsymbol{T}} - i|$ be the difference between the inclination i of the spacecraft and the inclination of the retrograde target orbit, $i_{\boldsymbol{T}} = |180\ \mathrm{deg} - i_T|$. Then $t = t_{1b}$ when $\Delta i_{\boldsymbol{T}} = 10$ deg. This means that at the end of phase 1, the sailcraft orbit does not have to be *exactly* retrograde, because this can be accounted for within phase 2.

Determination of the Optimal Orbit-Cranking Radius

If solar sail degradation is not considered, the acceleration capability of the solar sail increases $\propto 1/r^2$ when going closer to the sun. The minimum solar distance, however, is constrained by the temperature limit of the sail film T_{lim} and the spacecraft. Here, however, only the temperature limit of the sail film is considered. The equilibrium temperature of the sail film is [37]

$$T = \left[\frac{S_0}{\sigma}\frac{1-\rho}{\varepsilon_f + \varepsilon_b}\left(\frac{r_0}{r}\right)^2 \cos\alpha\right]^{1/4} \tag{3}$$

where $S_0 = 1368$ W is the solar constant, $\sigma = 5.67 \times 10^{-8}\ \mathrm{W \cdot m^{-2} \cdot K^{-4}}$ is the Stefan–Boltzmann constant, ρ is the front-side reflection coefficient of the sail film, ε_f and ε_b are the front- and back-side emission coefficients of the sail film, respectively, $r_0 = 1$ AU, and α is the light incidence angle or pitch angle. Thus, the sail temperature does not only depend on the solar distance, but also on the sail attitude, $T = T(r, \alpha)$ (and, of course, on the set of optical parameters $\mathcal{P}$ that is assumed as fixed within this paper). It was demonstrated in [38] that faster trajectories can be obtained for a given sail temperature limit T_{lim}, if not a minimum solar distance r_{lim}, but T_{lim} is used directly as a constraint. This can be realized by constraining the pitch angle α (that is also the light incidence angle) in a way that it cannot become smaller than the critical pitch angle, for which T_{lim} would be exceeded; that is, $\alpha > \alpha_{\mathrm{lim}}(r, T_{\mathrm{lim}})$.

Although orbit cranking is most effective for a circular orbit, it is also important to consider elliptic orbits. Therefore, we describe the optimal orbit-cranking behavior by an orbit-cranking semimajor axis a_{cr} instead of an orbit-cranking radius. Using the direct sail temperature constraint, a_{cr} defines the time Δt_{1b} that is required to make the orbit retrograde; Δt_{1b} is influenced by two adverse effects, leading to an optimal orbit-cranking semimajor axis $a_{\mathrm{cr,opt}}(T_{\mathrm{lim}})$, for which the inclination change rate $\Delta i/\Delta t$ is maximal and thus Δt_{1b} is minimal, as can be seen from Fig. 3. For $a_{\mathrm{cr}} < a_{\mathrm{cr,opt}}$, the inclination change takes longer than for $a_{\mathrm{cr,opt}}$ because of the lower SRP. For $a_{\mathrm{cr}} < a_{\mathrm{cr,opt}}$, the inclination change also takes longer than for $a_{\mathrm{cr,opt}}$ because of the (inefficiently) large critical pitch angle α_{lim} that is required to keep $T < T_{\mathrm{lim}}$; thus, $\Delta t_{1b} = \Delta t_{1b}(T_{\mathrm{lim}})$. It can seen from

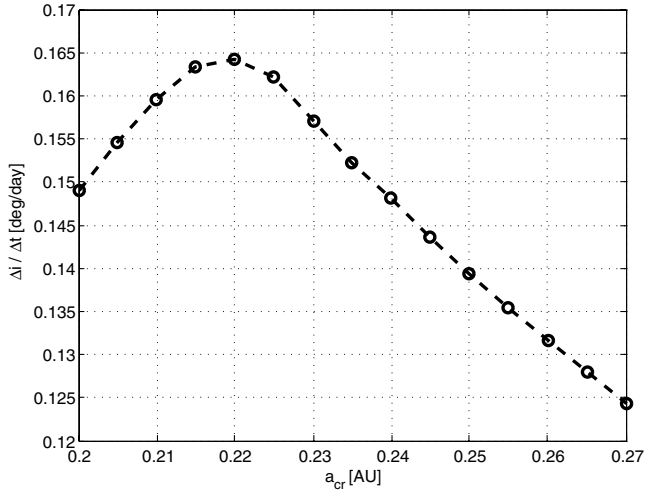

Fig. 3 Baseline mission scenario: dependence of inclination change rate on the orbit-cranking radius (circular orbit).

Fig. 3 that $a_{\mathrm{cr,opt}}(T_{\mathrm{lim}} = 240°\mathrm{C}) = 0.22$ AU, where $\Delta i/\Delta t = 0.1642$ deg/day.

Calculation of Phase 1 Using Local Steering Laws

Knowing now that the optimal semimajor axis for orbit cranking is 0.22 AU, we can calculate an estimate for Δt_1 using the local steering laws $\mathcal{L}_{a^-}$ (phase 1a, $\Rightarrow \Delta t_{1a}$) and $\mathcal{L}_{i^+}$ (phase 1b, $\Rightarrow \Delta t_{1b}$). The trajectories for both phases are shown in Figs. 4a and 4b. Figure 4c shows a very sharp transition between phases 1a and 1b. The time that is required for spiraling to $a_{\mathrm{cr,opt}}$ is $\Delta t_{1a} = 635.5$ days. If the final spacecraft state of phase 1a is taken as the initial spacecraft state for phase 1b, the time that is required for cranking the orbit to $\Delta i_T = 10$ deg is $\Delta t_{1b} = 973.5$ days. Therefore, the duration of phase 1 is $\Delta t_1 = 1609$ days. Note that this calculation did not include the alignment of the ascending node of the sailcraft Ω with the ascending node of the retrograde asteroid orbit Ω_T, and so $\Delta\Omega_T(t_{1b}) = |\Omega_T(t_{1b}) - \Omega(t_{1b})| = 56.7$ deg. This misalignment, however, could be removed by optimizing the launch date t_0. Note that when $\mathcal{L}_{a^-}$ is applied, the trajectory generally has some eccentricity at $a = a_{\mathrm{cr,opt}}$. If we do not use the final spacecraft state of phase 1a as the initial state for phase 1b, but assume a circular orbit to get the lower bound of what can be achieved with local steering laws, we get $\Delta t_{1b} = 960$ days for $\Delta i_T = 10$ deg, which is only 13.5 days less ($\Delta t_1 = 1595.5$ days).

Optimization of Phase 1 Using InTrance

Using InTrance, phase 1 is optimized in one pass. InTrance yields $\Delta t_1 = 1572$ days, which is 37 days (2.4%) faster than the LSL solution. Figure 5c now shows a very smooth transition between phases 1a and 1b. This result proves, as was already observed by Sauer [39], that a global optimal solution also tends to change the inclination during phase 1a whenever the solar sail is close to the nodes. Because of the poor *local* search behavior of InTrance, few "spikes" remain in the control angles (Fig. 5d), and so further fine-

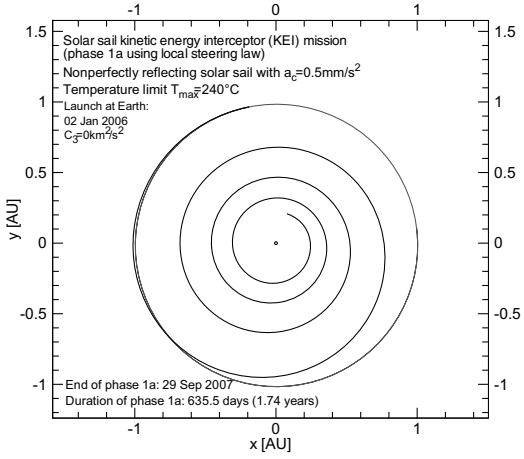

a) Trajectory for phase 1a

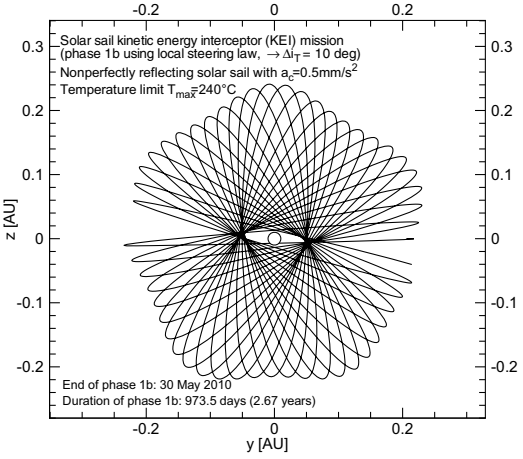

b) Trajectory for phase 1b

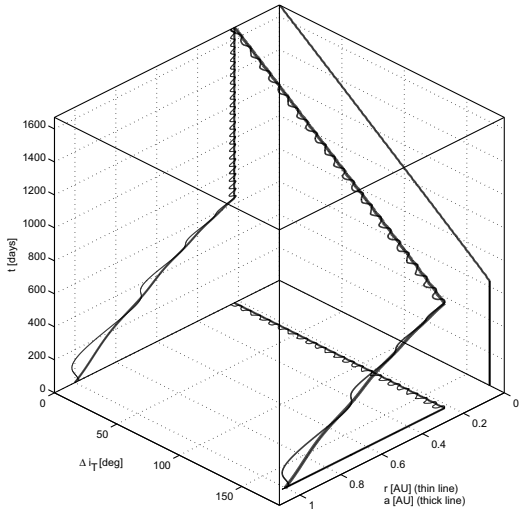

c) Δi_T-r-t-diagram

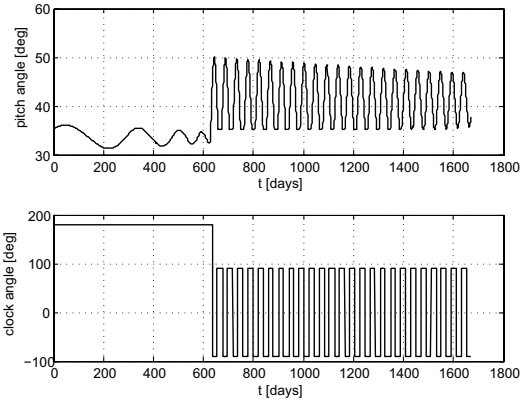

d) Steering angles

Fig. 4 Baseline mission scenario: phase 1, local steering law solution.

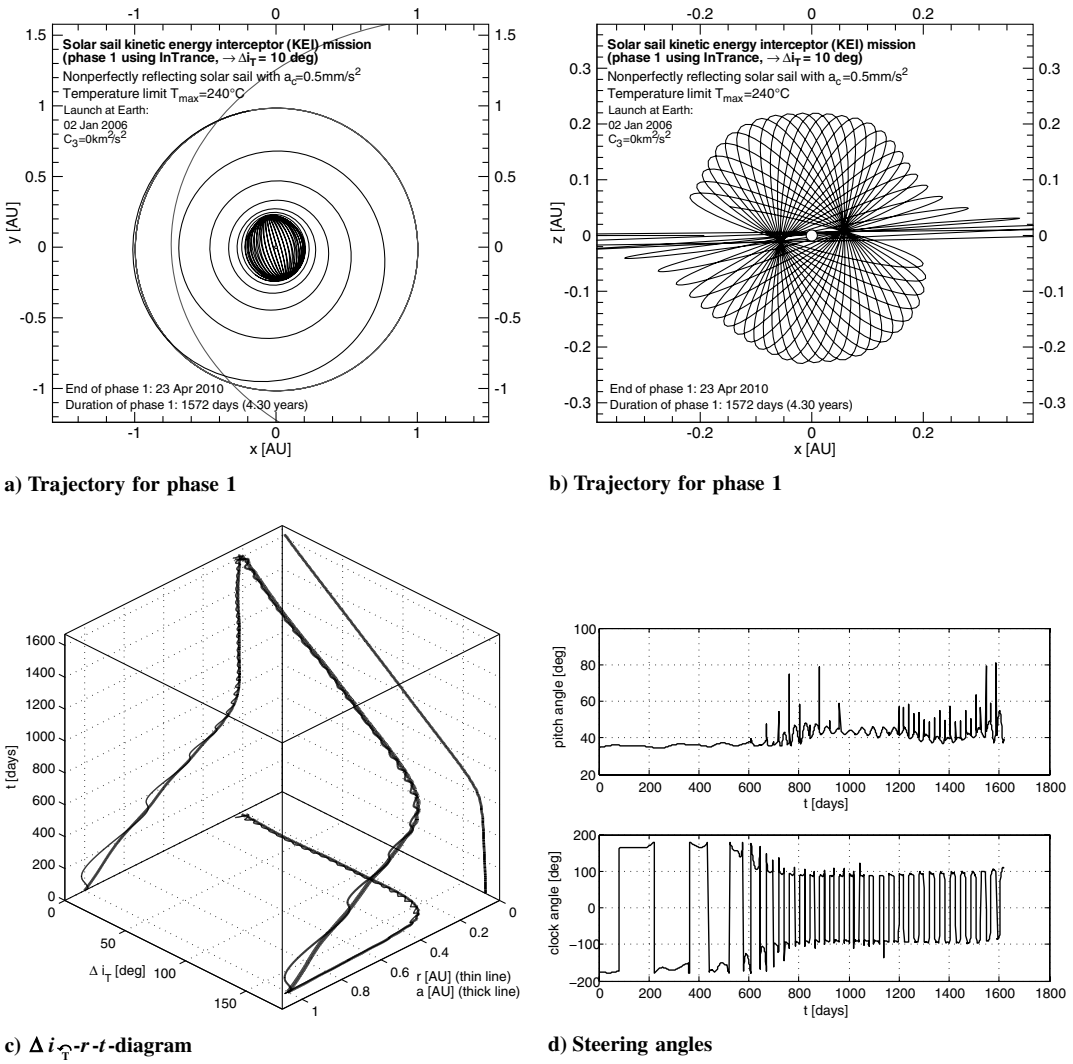

a) Trajectory for phase 1

b) Trajectory for phase 1

c) Δi_T-r-t-diagram

d) Steering angles

Fig. 5 Baseline mission scenario: phase 1, InTrance solution.

tuning of the solution might yield a shorter trajectory. The orientation of the final orbit is well aligned with the retrograde asteroid orbit, $\Delta\Omega_{\boldsymbol{T}}(t_{1b}) = 1.3$ deg.

Optimization of Phase 1 Using a Combination of InTrance and $\mathcal{L}_{i^+}$

Looking at Fig. 5c, one sees that a_{cr} is not constant during phase 1b. In addition to the spikes in the control angles (Fig. 5d), this also indicates that the InTrance solution is not locally optimal. Therefore, we have applied a combination of InTrance with the local steering law $\mathcal{L}_{i^+}$, using InTrance until $a = a_{\mathrm{cr,opt}}$ and $\mathcal{L}_{i^+}$, from this point on. The results are shown in Fig. 6. This strategy yields $\Delta t_1 = 1564$ days, showing that the InTrance solution for phase 1b was suboptimal, however, only very slightly (8 days, 0.5%). The orientation of the final orbit is well aligned with the retrograde asteroid orbit, $\Delta\Omega_{\boldsymbol{T}}(t_{1b}) = 1.5$ deg.

Optimization of Phase 2

For the following calculations, it is assumed that a head-on collision with a relative velocity $v_{\mathrm{imp}} = 70$ km/s at the asteroid's perihelion leads to a change of the asteroid's orbital velocity of $\Delta v_{\mathrm{NEA,imp}} = 0.3$ cm/s (see [14]). Thus, assuming that $\Delta v_{\mathrm{NEA,imp}}$ varies proportional to v_{imp}, we can assume (for simplicity, without further impact modeling) a collision efficiency factor of $\Delta v_{\mathrm{NEA,imp}}/v_{\mathrm{imp}} = 4.3 \times 10^{-8}$. Therefore, the goal of phase 2 is to maximize the head-on impact velocity. The optimization objective used for InTrance was to maximize $\boldsymbol{v} \cdot (-\boldsymbol{v}_{\mathrm{NEA}})$! Figure 7 shows the resulting trajectory and the orbital elements that define the shape and inclination of the orbit.

InTrance achieves an impact velocity of 81.4 km/s. This yields $\Delta v_{\mathrm{NEA,imp}} = 0.349$ cm/s. Numerical integration of the asteroid's orbit after the impact, including all planetary disturbances, yields a deflection distance of $\Delta r_{\mathrm{defl}} = 4656$ km (0.73 Earth radii) on 14 January 2015, the date of Earth impact. Note that the deflection is larger than would be obtained with Eq. (1), due to a close Mars flyby of the asteroid after the KEI impacts. It is clear that the impact velocity depends only on the characteristic acceleration of the sailcraft and the time Δt_2 that is available after phase 1 to maximize the impact velocity; thus, $v_{\mathrm{imp}} = v_{\mathrm{imp}}(a_c, \Delta t_2)$. Having evaluated several postimpact calculations, the deflection distance (for this scenario) can be approximated with an error of less than 0.1% (with the assumptions of the impact model) by

$$\widetilde{\Delta r_{\mathrm{defl}}} \approx 57.16 \cdot \tilde{v}_{\mathrm{imp}} \tag{4}$$

where the tilde denotes the dimensionless variables $\widetilde{\Delta r_{\mathrm{defl}}} = \Delta r_{\mathrm{defl}}/1$ km and $\tilde{v}_{\mathrm{imp}} = v_{\mathrm{imp}}/(1$ km/s).

Variation of the Hyperbolic Excess Energy for Interplanetary Insertion

In this section, the influence of the hyperbolic excess energy C_3 on the mission performance is investigated. To find out how C_3 influences the time that is available for phase 2 to gain orbital energy, we have used InTrance to calculate $\Delta t_1(C_3)$. This then gives

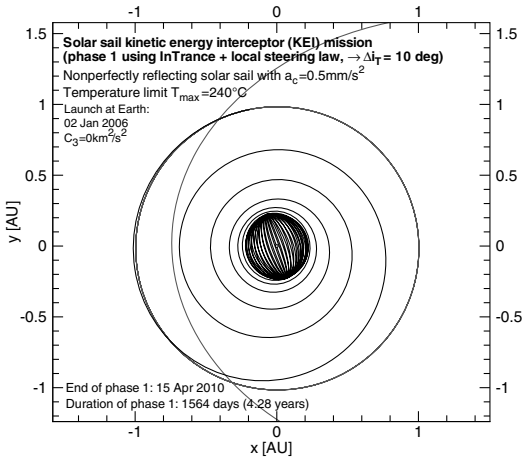

a) Trajectory for phase 1

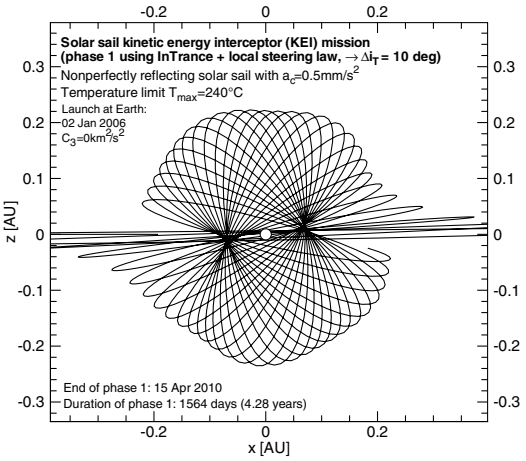

b) Trajectory for phase 1

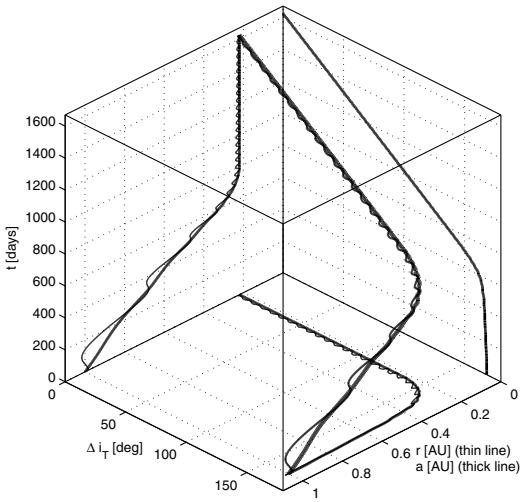

c) Δi_T-r-t-diagram

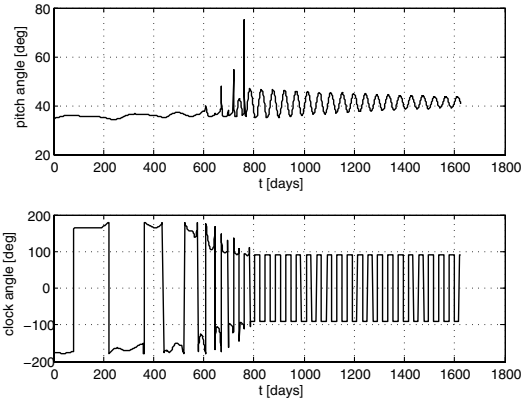

d) Steering angles

Fig. 6 Baseline mission scenario: phase 1, combination of InTrance solution and local steering law.

$\Delta t_2(C_3) = \Delta t - \Delta t_1(C_3)$. The results are shown in Fig. 8a. As expected, the time that is available for phase 2 increases with C_3. For $0\ \text{km}^2/\text{s}^2 \le C_3 \le 100\ \text{km}^2/\text{s}^2$, it can be approximated with an error of less than 10% by

$$\widetilde{\Delta t_2} = 626 + 68.5 \cdot \tilde{C}_3^{0.4} \tag{5}$$

where $\widetilde{\Delta t_2} = \Delta t_2/1\,\text{day}$ and $\tilde{C}_3 = C_3/(1\ \text{km}^2/\text{s}^2)$. We have also investigated how the time that is available for phase 2 influences the

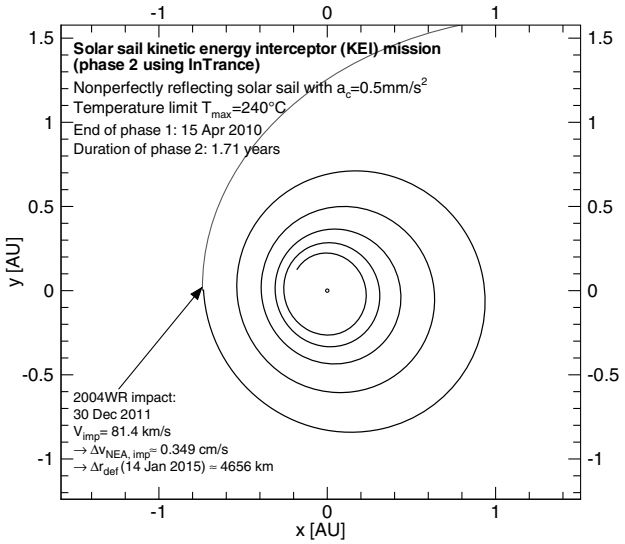

a) Trajectory for phase 2

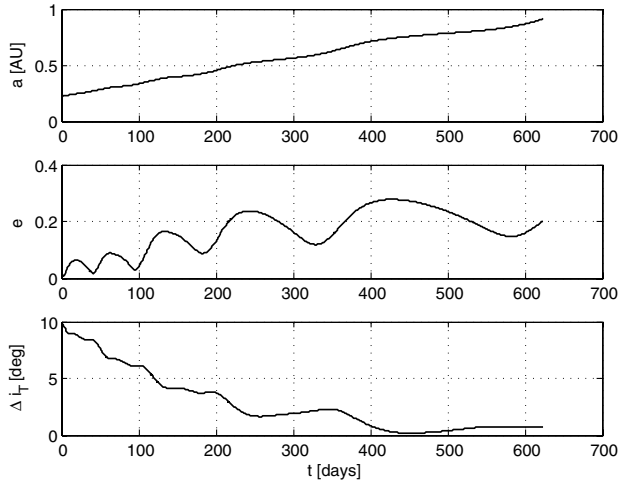

b) Selected orbital elements

Fig. 7 Baseline mission scenario: phase 2, InTrance solution.

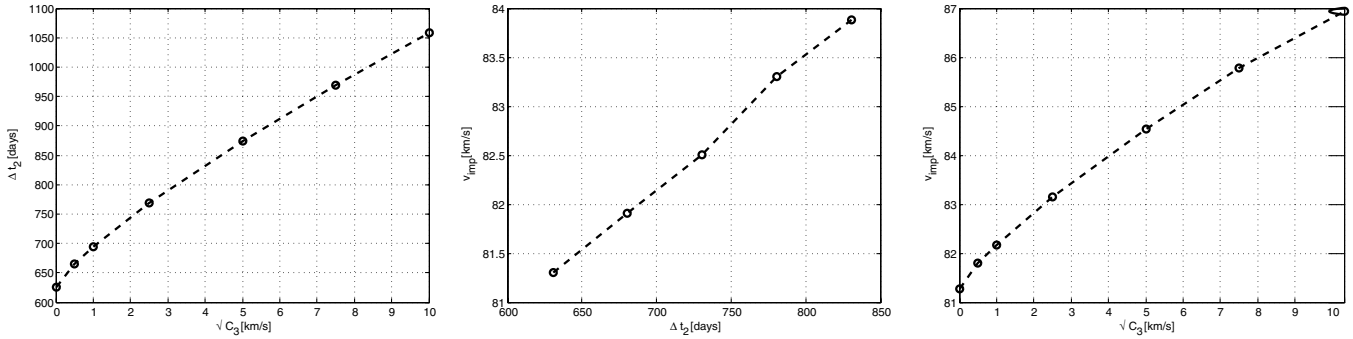

a) Δt_2 **over** C_3 **b)** v_{imp} **over** Δt_2 **c)** v_{imp} **over** C_3

Fig. 8 Variation of C_3 ($a_c = 0.5$ mm/s^2 and $T_{\text{lim}} = 240$°C).

impact velocity. For this purpose, we have taken the spacecraft state of the reference trajectory at t_{1b} as the initial state for phase 2, but set the date back by 50, 100, 150, and 200 days, so that this time is additionally available for the sail to gain orbital energy for the impact. The results are shown in Fig. 8b. As expected, the impact velocity increases with the duration of phase 2. For 600 days $\lesssim \Delta t_2 \lesssim$ 850 days, it can be approximated with an error of less than 0.1% by

$$\tilde{v}_{\text{imp}} \approx 73.017 + 0.0131 \cdot \widetilde{\Delta t_2} \tag{6}$$

Combining Eqs. (5) and (6), we can approximate the impact velocity for 0 km^2/s$^2 \lesssim C_3 \lesssim$ 25 km^2/s^2 by

$$\tilde{v}_{\text{imp}} \approx 81.218 + 0.897 \cdot \tilde{C}_3^{0.4} \tag{7}$$

Variation of the Sail Temperature Limit

In this section, the influence of the solar sail temperature limit T_{lim} on the mission performance is investigated. Figure 9 shows, for a circular orbit, $(\Delta i/\Delta t)(a_{\text{cr}})$ for different solar sail temperature limits. For 200°C $\le T_{\text{lim}} \le$ 260°C, the optimal orbit-cranking semimajor axis can be approximated with an error of less than 1% by

$$\tilde{a}_{\text{cr,opt}} \approx 30 \cdot \tilde{T}_{\text{lim}}^{-0.897} \tag{8}$$

where $\tilde{a}_{\text{cr,opt}} = a_{\text{cr,opt}}/1\,\text{AU}$ and $\tilde{T}_{\text{lim}} = T_{\text{lim}}/1°\text{C}$. The maximum inclination change rate can be approximated with an error of less than 1% by

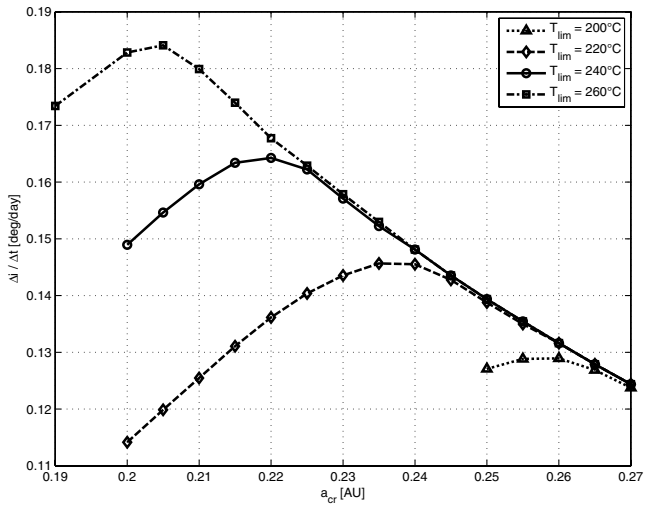

Fig. 9 Dependence of the inclination change rate on the orbit-cranking radius for different solar sail temperature limits (circular orbit).

$$(\widetilde{\Delta i/\Delta t})_{\max} \approx 9.26 \times 10^{-4} \cdot \tilde{T}_{\text{lim}} - 5.68 \times 10^{-2} \tag{9}$$

where $(\widetilde{\Delta i/\Delta t})_{\max} = (\Delta i/\Delta t)_{\max}/(1\ \text{deg/day})$.

We used InTrance to optimize phase 1 for different solar sail temperature limits (200°C $\le T_{\text{lim}} \le$ 260°C). The results are shown in Table 1 and Fig. 10. Figure 10b shows that InTrance very closely matches the optimal orbit-cranking semimajor axes shown in Fig. 9. For 200°C $\le T_{\text{lim}} \le$ 260°C, the time required for phase 1 can be approximated with an error of less than 1% by

$$\widetilde{\Delta t_1} \approx 8.05 \times 10^4 \cdot \tilde{T}_{\text{lim}}^{-0.718} \tag{10}$$

and so the time that is available for phase 2 can be approximated by

$$\widetilde{\Delta t_2} \approx 2190 - 8.05 \times 10^4 \cdot \tilde{T}_{\text{lim}}^{-0.718} \tag{11}$$

Using Eq. (6), the impact velocity can then be approximated (with an error of less than 0.25%) by

$$\tilde{v}_{\text{imp}} \approx 101.7 - 1055 \cdot \tilde{T}_{\text{lim}}^{-0.718} \tag{12}$$

Variation of the Characteristic Acceleration

In this section, the influence of the characteristic acceleration a_c on the mission performance is investigated. We used InTrance to optimize phase 1 for different characteristic accelerations (0.5 mm/s$^2 \le a_c \le$ 0.6 mm/s^2). The results are shown in Table 2 and Fig. 11. Figure 11b shows that the optimal orbit-cranking semimajor axis is independent of a_c. For 0.5 mm/s$^2 \le a_c \le$ 0.6 mm/s^2, the maximum inclination change rate can be approximated with an error of less than 0.1% by

$$(\widetilde{\Delta i/\Delta t})_{\max} \approx 0.3238 \cdot \tilde{a}_c^{0.9794} \tag{13}$$

where $\tilde{a}_c = a_c/(1\ \text{mm/s}^2)$. The duration of phase 1 can then be approximated with an error of less than 0.4% by

$$\widetilde{\Delta t_1} \approx 297.1 \cdot \tilde{a}_c^{-0.8257} + \frac{170}{0.3238 \cdot \tilde{a}_c^{0.9794}} \approx 297.1 \cdot \tilde{a}_c^{-0.8257} + 525 \cdot \tilde{a}_c^{-0.9794} \tag{14}$$

The duration of phase 2 is then approximately

Table 1 Variation of T_{lim} ($a_c = 0.5$ mm/s^2, $C_3 = 0$ km^2/s^2, InTrance, and $\mathcal{L}_{i^+}$).

T_{lim}, °C	$a_{\text{cr,opt}}$, AU	$(\Delta i/\Delta t)_{\max}$, deg/day	Δt_1	Δt_2	$\tilde{v}_{\text{imp}}$	$\widetilde{\Delta r_{\text{defl}}}$
200	0.260	0.1291	1806	384	78.0	4460
220	0.236	0.1461	1661	529	79.9	4570
240	0.220	0.1648	1564	626	81.2	4640
260	0.205	0.1838	1494	696	82.1	4690

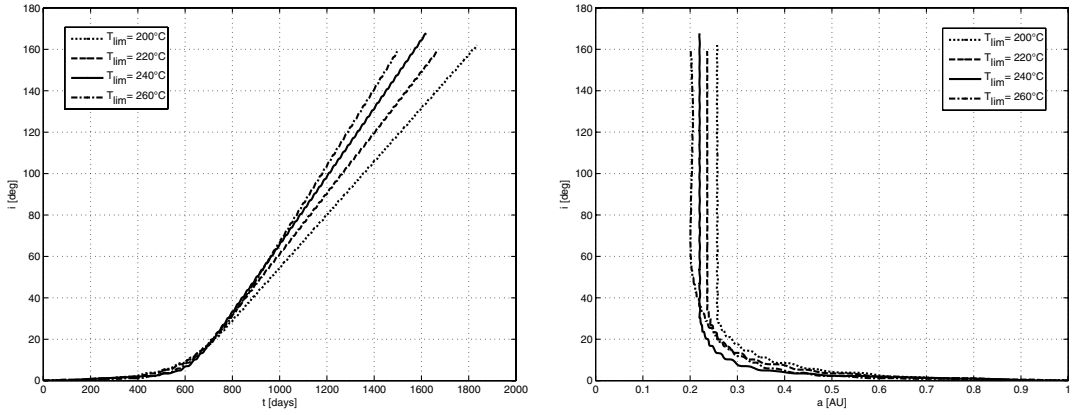

a) Inclination over flight time, $i(t)$ b) Inclination over semimajor axis, $i(a)$

Fig. 10 Phase 1, optimized with InTrance: variation of $T_{\lim}$ ($a_c = 0.5$ mm/s^2 and $C_3 = 0$ km^2/s^2).

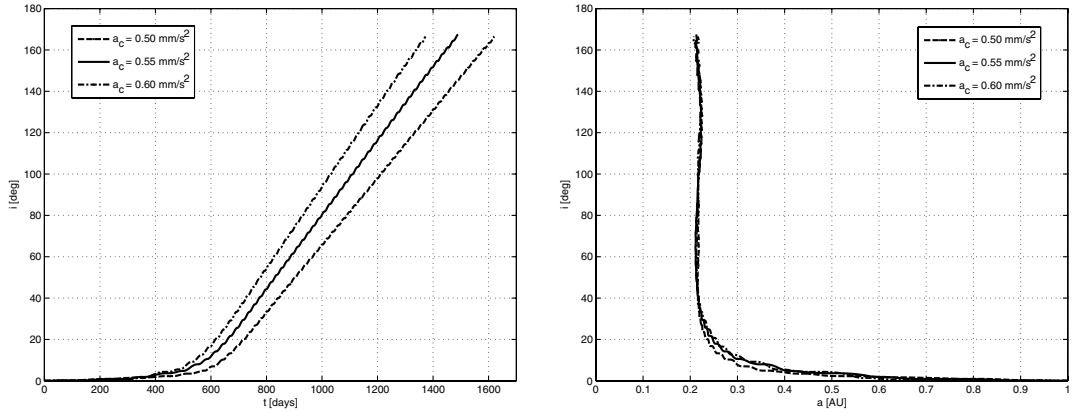

a) Inclination over flight time, $i(t)$ b) Inclination over semimajor axis, $i(a)$

Fig. 11 Phase 1, optimized with InTrance: variation of a_c ($T_{\lim} = 240$°C and $C_3 = 0$ km^2/s^2).

$$\widetilde{\Delta t_2} \approx 2190 - 297.1 \cdot \tilde{a}_c^{-0.8257} - 525 \cdot \tilde{a}_c^{-0.9794} \qquad (15)$$

Solar Sail Degradation

To investigate the effects of optical degradation of the sail film, as is expected in the extreme space environment close to the sun, we now apply the parametric model developed in [30]. In this parametric model, the optical parameters p are assumed to depend on the cumulated solar radiation dose (SRD) $\sum(t)$ on the sail. The (dimensionless) SRD is

$$\sum(t) = \frac{\tilde{\sum}(t)}{\tilde{\sum}_0} = \left(r_0^2 \int_{t_0}^{t} \frac{\cos\alpha}{r^2}\, \mathrm{d}t' \right) \Big/ 1 \text{ year} \qquad (16)$$

with $\tilde{\sum}_0 \triangleq S_0 \cdot 1$ year $= 1368$ W/m$^2 \cdot 1$ year $= 15.768$ TJ/m^2 being the annual SRD on a surface perpendicular to the sun at 1 AU. The degradation constant λ is related to the "half-life solar radiation dose" $\hat{\sum}$ [$\sum = \hat{\sum} \Rightarrow p = 1/2 \cdot (p_0 + p_\infty)$] via $\lambda = \ell_n\, 2/\hat{\sum}$. The degradation factor d defines the end-of-life values p_∞ of the optical parameters. Table 3 and Fig. 12 show the results for different degradation factors $0 \le d \le 0.2$, assuming a half-life SRD of $25 S_0 \cdot 1$ year $= 394$ TJ/m^2. It can be seen from Table 3 that for $d > 0.05$, it is not possible to meet the mission objective. The time that is available for phase 2 is too short to make an impact with the target. Figure 12b shows that for larger degradation factors, it is favorable to make the orbit cranking further away from the sun than would be optimal without degradation. The main degradation effect can be seen from Fig. 12a, which shows that $\Delta i/\Delta t$ becomes smaller with increasing SRD. Because the underestimation of optical degradation could be a show-stopper for this mission, and because the real degradation behavior of solar sails in the space environment is (to a considerable degree) indefinite, extensive ground and in-space tests are required before this mission.

Table 2 Variation of a_c ($T_{\lim} = 240$°C, $C_3 = 0$ km^2/s^2, InTrance, and $\mathcal{L}_{i^+}$)

a_c, mm/s^2	$(\Delta i/\Delta t)_{\max}$, deg/day	Δt_1, days	Δt_2, days	$\tilde{v}_{\text{imp}}$, km/s	Δr_{defl}, km
0.5	0.1642	1564	626	81.4	4656
0.55	0.1803	1425	765	83.8	4791
0.6	0.1963	1323	867	85.0	4857

Table 3 Variation of the optical degradation factor (InTrance)

d	Δt_1, days	Δt_2, days	v_{imp}, km/s	Δr_{defl}, km
0.0	1572	618	81.4	4640
0.05	1705	485	79.4	4540
0.1	1839	351	——	——
0.2	2074	116	——	——

Conclusions

We showed that solar sails are a realistic option to deflect a fictional 200-m diameter asteroid with a kinetic impact. The required technology for such a mission, however, is not yet state of the art, but would have to be developed in a sharply pursued technological program within the next 20 years. In our baseline scenario, we used a nonperfectly reflecting solar sail with a maximum acceleration of 0.5 mm/s^2 at 1 AU to transport a separable 150-kg impactor to the target within six years. A sail temperature limit of 240°C was

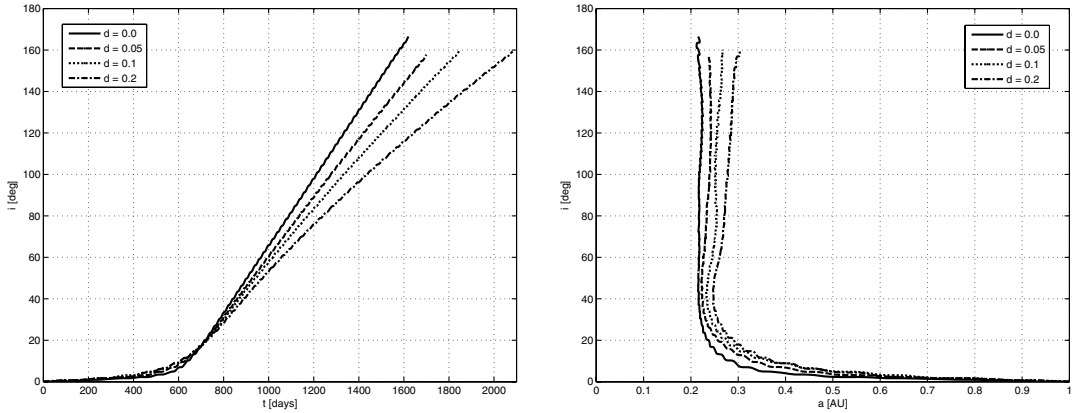

a) Inclination over flight time, $i(t)$ **b) Inclination over semimajor axis, $i(a)$**

Fig. 12 Phase 1, optimized with InTrance: different optical degradation factors ($a_c = 0.5$ mm/s^2, $T_{\lim} = 240°$C, and $C_3 = 0$ km^2/s^2).

assumed and zero hyperbolic excess energy for interplanetary insertion. We showed that such a sailcraft is able to impact the asteroid with a relative head-on velocity of 81.4 km/s at its perihelion, leading to an estimated deflection of more than a half-Earth radius. The impact velocity can be increased by a considerable amount, either by using a lighter solar sail, by using a more temperature-resistant sail, or by inserting the sailcraft with a larger hyperbolic excess velocity at Earth. We also found that the mission performance might be seriously affected by optical degradation of the sail surface, as is expected in the extreme space environment close to the sun. However, because the real degradation behavior of solar sails in the space environment is (to a considerable degree) indefinite, ground and in-space tests are required before this mission. Other problems that have to be considered for the design of this mission are the extreme requirements for the terminal guidance before impact (accuracy much better than 100 m at a relative velocity of more than 80 km/s) and the thermal control that has to withstand very close solar distances (0.2–0.25 AU).

Acknowledgments

The constructive comments of Malcolm Macdonald and Ian Carnelli on the manuscript are greatly appreciated.

References

[1] "European Asteroid Research Node," *The Near-Asteroids Data Base* [online database], http://earn.dlr.de/nea/ [retrieved 28 Sept. 2006].

[2] Anon., "The Exploration of Near-Earth Objects," Committee on Planetary and Lunar Exploration, Space Studies Board, National Research Council, Washington, D.C., 1998.

[3] Rampino, M., and Haggerty, B., "Extraterrestrial Impacts and Mass Extinctions of Life," *Hazards Due to Comets and Asteroids*, edited by T. Gehrels, Univ. of Arizona Press, Tucson, AZ, 1994, pp. 827–857.

[4] Ward, P., and Brownlee, D., *Rare Earth. Why Complex Life Is Uncommon in the Universe*, Copernicus, New York, 2000.

[5] Morrison, D., Chapman, C., and Slovic, P., "The Impact Hazard," *Hazards Due to Comets and Asteroids*, edited by T. Gehrels, Univ. of Arizona Press, Tucson, AZ, 1994, pp. 59–91.

[6] Hills, J., Nemchinov, I., Popov, S., and Teterev, A., "Tsunami Generated by Small Asteroid Impacts," *Hazards Due to Comets and Asteroids*, edited by T. Gehrels, Univ. of Arizona Press, Tucson, AZ, 1994, pp. 779–789.

[7] Bottke, W., Nolan, M., Greenberg, R., and Kolvoord, R., "Collisional Lifetimes and Impact Statistics of Near-Earth Asteroids," *Hazards Due to Comets and Asteroids*, edited by T. Gehrels, Univ. of Arizona Press, Tucson, AZ, 1994, pp. 337–357.

[8] Gladman, B., Michel, P., and Froeschle, C., "The Near-Earth Object Population," *Icarus*, Vol. 146, No. 1, 2000, pp. 176–189.

[9] De Pater, I., and Lissauer, J., *Planetary Sciences*, Cambridge Univ. Press, New York, 2001.

[10] Chesley, S., "Potential Impact Detection for Near-Earth Asteroids: The Case of 99942 Apophis (2004 MN4)," *Asteroids, Comets, Meteors. Proceedings IAU Symposium No. 229*, edited by S. Ferraz-Mello and D. Lazzaro, Cambridge Univ. Press, New York, 2006.

[11] Gehrels, T. (ed.), *Deflection and Fragmentation of Near-Earth Asteroids*, Univ. of Arizona Press, Tucson, AZ, 1994.

[12] Gold, R., "SHIELD: A Comprehensive Earth Protection System," NASA Institute for Advanced Concepts, Rept. SDO-10974, 1999.

[13] Housen, R., and Holsapple, K., "Impact Cratering on Porous Asteroids," *Icarus*, Vol. 163, No. 1, 2003, pp. 102–119.

[14] Wie, B., "Solar Sailing Kinetic Energy Interceptor (KEI) Mission for Impacting/ Deflecting Near-Earth Asteroids," 41st AIAA/ASME/SAE/ASEE Joint Propulsion Conference and Exhibit, Tucson, AZ, AIAA Paper 2005-3725, July 2005.

[15] McInnes, C., "Deflection of Near-Earth Asteroids by Kinetic Energy Impacts From Retrograde Orbits," *Planetary and Space Science*, Vol. 52, No. 7, 2004, pp. 587–590.

[16] McInnes, C., Hughes, G., and Macdonald, M., "High-Energy Small Body Missions Using Solar Sail Propulsion," 56th International Astronautical Congress, Fukuoka, Japan, International Astronautical Congress, Paper 05-A3.5.B, Oct. 2005.

[17] Wie, B., "Thrust Vector Control of Solar Sail Spacecraft," AIAA Guidance, Navigation, and Control Conference, San Francisco, CA, AIAA Paper 2005-6086, Aug. 2005.

[18] Dachwald, B., and Wie, B., "Solar Sail Trajectory Optimization for Intercepting, Impacting, and Deflecting Near-Earth Asteroids," *Journal of Spacecraft and Rockets* (submitted for publication); also AIAA Guidance, Navigation, and Control Conference, San Francisco, CA, AIAA Paper 2005-6176, Aug. 2005.

[19] Blume, W., "Deep Impact: Mission Design Approach for a New Discovery Mission," *Acta Astronautica*, Vol. 52, Nos. 2–6, 2003, pp. 105–110.

[20] Carnelli, I., Gàlvez, A., and Ongaro, F., "Learning to Deflect Near-Earth Objects: Industrial Design of the Don Quijote Mission" 57th International Astronautical Congress, Valencia, Spain, International Astronautical Congress Paper IAC06-A3.5.5, Oct. 2006.

[21] Garbe, G., and Montgomery, E., "An Overview of NASA's Solar Sail Propulsion Project," 39th AIAA/ASME/SAE/ASEE Joint Propulsion Conference and Exhibit, Huntsville, AL, AIAA Paper 2003-4662, July 2003.

[22] Murphy, D., Murphy, T., and Gierow, P., "Scalable Solar-Sail Subsystem Design Concept," *Journal of Spacecraft and Rockets*, Vol. 40, No. 4, 2003, pp. 539–547.

[23] Wie, B., "Solar Sail Attitude Control and Dynamics, Part 1," *Journal of Guidance, Control, and Dynamics*, Vol. 27, No. 4, 2004, pp. 526–535.

[24] Wie, B., "Solar Sail Attitude Control and Dynamics, Part 2," *Journal of Guidance, Control, and Dynamics*, Vol. 27, No. 4, 2004, pp. 536–544.

[25] Murphy, D., and Wie, B., "Robust Thrust Control Authority for a Scalable Sailcraft," *Spaceflight Mechanics 2004*, edited by S. Coffey, A. Mazzoleni, K. Luu, and R. Glover, Vol. 119, Advances in the Astronautical Sciences, Part 3, Univelt, Inc., San Diego, CA, 2004, pp. 2909–2928.

[26] Wie, B., Murphy, D., Thomas, S., and Paluszek, M., "Robust Attitude Control Systems Design for Solar Sails, Part 1: Propellantless Primary ACS," AIAA Paper 2004-5010, Aug. 2004.

[27] Wie, B., Murphy, D., Thomas, S., and Paluszek, M., "Robust Attitude Control Systems Design for Solar Sails, Part 2: MicroPPT-based Backup ACS," AIAA Paper 2004-5011, Aug. 2004.

[28] Wie, B., Thomas, S., Paluszek, M., and Murphy, D., "Propellantless AOCS Design for a 160-m, 450-kg Sailcraft of the Solar Polar Imager Mission," AIAA Paper 2005-3928, July 2005.

[29] Wright, J., *Space Sailing*, Gordon and Breach, Philadelphia, 1992.

[30] Dachwald, B., Mengali, G., Quarta, A., and Macdonald, M., "Parametric Model and Optimal Control of Solar Sails with Optical Degradation," *Journal of Guidance, Control, and Dynamics*, Vol. 29, No. 5, 2006, pp. 1170–1178.

[31] Dachwald, B., "Low-Thrust Trajectory Optimization and Interplanetary Mission Analysis Using Evolutionary Neurocontrol," Ph.D. Thesis, Universität der Bundeswehr München, Neubiberg, Germany, 2004.

[32] Dachwald, B., "Optimization of Interplanetary Solar Sailcraft Trajectories Using Evolutionary Neurocontrol," *Journal of Guidance, Control, and Dynamics*, Vol. 27, No. 1, 2004, pp. 66–72.

[33] Dachwald, B., "Optimization of Very-Low-Thrust Trajectories Using Evolutionary Neurocontrol," *Acta Astronautica*, Vol. 57, Nos. 2–8, 2005, pp. 175–185.

[34] Wright, J., "Solar Sailing: Evaluation of Concept and Potential," Battelle Columbus Labs., Rept. BMI-NLVP-TM-74-3, Columbus, OH, Mar. 1976.

[35] Wright, J., and Warmke, J., "Solar Sail Mission Applications," AIAA Paper 76-808, Aug. 1976.

[36] Sauer, C., "A Comparison of Solar Sail and Ion Drive Trajectories for a Halley's Comet Rendezvous Mission," American Astronautical Society Paper 77-104, Sept. 1977.

[37] McInnes, C., *Solar Sailing: Technology, Dynamics and Mission Applications*, Springer–Praxis Series in Space Science and Technology, Springer–Praxis, New York, 1999.

[38] Dachwald, B., "Optimal Solar Sail Trajectories for Missions to the Outer Solar System," *Journal of Guidance, Control, and Dynamics*, Vol. 28, No. 6, 2005, pp. 1187–1193.

[39] Sauer, C., "Solar Sail Trajectories for Solar-Polar and Interstellar Probe Missions," *Astrodynamics 1999*, Vol. 103, edited by K. Howell, F. Hoots, and B. Kaufman, Advances in the Astronautical Sciences, Univelt, Inc., San Diego, CA, 2000, pp. 547–562.

D. Edwards
Associate Editor